An Improved Multiline Analysis for Monolithic Inductors

Morin Dehan, Jean-Pierre Raskin, *Member, IEEE*, Isabelle Huynen, *Member, IEEE*, and Danielle Vanhoenacker-Janvier, *Senior Member, IEEE*

***Abstract*—This paper presents a new efficient multiline model for monolithic inductors. A preliminary model was developed by Huynen, which divided the spiral in sections of coupled transmission lines whose parameters are calculated by a variational principle. This model has been improved for inductors with high trace width-to-gap ratios and it has been demonstrated to be adequate for predicting S-parameters characterizing the inductor over a wide frequency band, even above its self-resonant frequency. This new design tool is shown to be useful for analyzing and optimizing inductor topologies built on both insulating and semiconducting substrates.**

***Index Terms*—Inductor model, integrated circuit (IC) modeling, substrate loss.**

I. Introduction

THE boom in mobile communications has led to an increasing desire for low-cost and low-power mixed-mode integrated circuits (ICs). A very high degree of integration, a lower power consumption, and the use of a lower supply voltage are the goals set for new developments in wireless transceiver design. Present-day transceivers often consist of a three or four chip-set solution combined with several external components. The required number of external components is linked to the physical limitations of the analog front-end topology. A further reduction of the number of external components is essential to obtain a lower cost, power consumption, and weight. The evolution of wireless transceiver design will be the realization of the complete transceiver (analog and digital processing) on one chip.

Submicrometer CMOS technology appears to be a feasible and cost-effective integration solution for mobile communication systems. Effectively, the maturity of silicon-based CMOS technology for small device feature size and low-voltage digital circuits and also the recent progresses of MOSFET's microwave performances [1]–[5] explain the silicon success compared to III–V technologies. Unfortunately, the fabrication of high-quality passive elements is quite difficult due to two major limitations of silicon-based technologies, which are the relatively high losses linked to the silicon substrate itself and the relatively thin metal layers used for interconnections. However, several solutions have been presented recently in the literature to overcome those limitations, and experimental results have shown the possibility reaching high quality factor (>30) for inductors integrated on silicon substrates. The main proposed solutions to overcome the parasitic substrate effects are the use of high-resistivity silicon substrates [6], a very thick buried oxide layer [7], or a porous silicon region [8] underneath the inductors, the silicon substrate removal below the inductor area by micromachining techniques [9], [10], and the use of a patterned ground shield [11]. Thicker metallization and stacking of multiple metal layers are used to reduce the conductor dissipation [12]. Design guidelines have been proposed to optimize the geometric parameters of microstrip spiral inductors, such as strip width, spacing between the strips, and the gap between groups of coupled lines on opposing sides (the hole at the middle of the spiral inductor) [13], [10]. Despite these technical improvements, only a few successful RF analog circuits have been reported in the literature [14]–[18]. The slow emergence of CMOS technologies into the market of RF circuits is in part linked to the lack of accurate and rapid simulation tools for passive elements.

The classical RF and microwave models available for the integrated inductors are of various types. We can divide the computer-aided design (CAD) for spiral inductors into: 1) the full-wave electromagnetic simulators (EMSs) category and the 2) simple π-model category for which the lumped-element values are determined by semiempirical equations or by using fitting techniques on high-frequency measurements. EMS simulators based on two-dimensional (2-D) or three-dimensional (3-D) modeling of the element use a spectral-domain approach [19], the method of moments [20], the method of lines [21], or a finite-element method [22]. The computation time, however, is reported to increase with the number of turns, losses into the substrate, and the ratio linewidth (W) to line spacing (S), and becomes rapidly too large for online design and optimization. Lumped-element models and also tables of measured data (introduced in the circuit simulator as a black box) are usually preferred to complex distributed models by monolithic-microwave integrated-circuit (MMIC) designers because they are easy to introduce into commercial circuit simulators and, moreover, they do not increase the computation time of circuit optimization. The parameters of the equivalent circuit are extracted and validated by measuring a series of inductors of various geometries [23]–[25]. However, these models suffer from various limitations: they are not valid above the resonant frequency (thus, not suitable for accurate simulations of nonlinear circuits), they are generally scalable versus some parameters (not all of them), and they are only accurate for the technology, type of substrate, range of dimensions of

Manuscript received June 21, 2001; revised May 10, 2002. This work was supported in part by the Communauté Française de Beigique under the Actions de Recherche Concertées Program and by the European Committee (EEC) under the ESPRIT Project.

The authors are with the Microwave Laboratory, Université catholique de Louvain, B-1348 Louvain-la-Neuve, Belgium (e-mail: dehan@emic.ucl.ac.be).

Digital Object Identifier 10.1109/TMTT.2002.806922

the measured inductors, and measurement's frequency range. Concerning the use of tables of measured data for inductors, this is a practical tool for RF designers to optimize the circuit performances for a fixed inductor design, but it cannot be used for the optimization of the inductor design itself.

In order to overcome some of these limitations, an efficient design method has been developed by Huynen for MMIC inductors [26]. It requires only the geometry of the spiral inductor and the electrical parameters of the substrate as input parameters and, as a consequence, can be used with the same accuracy for various technologies and topologies of inductors. This model was developed for inductances with low linewidth to line spacing ratio (W/S). This preliminary model [26] is extended and optimized in this paper for inductors with high trace width-to-gap ratios.

The geometrical and technological parameters of inductors analyzed in this paper are described in Section II. Sections III and IV briefly describe the preliminary model [26] of the integrated inductor, as well as its efficiency and limitations. Section V shows how it is possible to optimize the model for high W/S values, and Section VI validates the model for inductors on moderate-resistivity silicon (20 $\Omega \cdot$ cm) and high-resistivity quartz substrates.

II. Inductor Geometries

In Fig. 1, the top view and cross section for the spiral inductors studied in this paper are shown. Each microstrip spiral is fabricated using 2-μm-thick aluminum with 10-Ω/sq sheet resistance. A 1-μm-thick underpass is used to contact the center of the spiral to the pad access for measurement purpose. The spiral is separated from the underpass line and the silicon or quartz substrate by oxide layers of 2 μm (t_{uox}) and 4 μm (t_{ox}), respectively. Table I presents the geometrical dimensions of the various inductors for which the simulation and experimental results are analyzed and discussed in this paper.

III. Description of the Preliminary Model

The model described in here is a transmission-line model. For solving the multiline analysis, the spiral is first divided into sections of n-coupled lines, "n" varying with the position in the spiral. Each strip in the section is supposed to be influenced by the two adjacent strips only (then C_{m2} and L_{m2} in Fig. 2 are neglected) and the parameters of the coupled lines are the (L, C) elements of a single line and the mutual capacitance and inductance (C_m, L_m) of the adjacent lines. The line parameters are calculated by using a variational formalism, taking into account the geometrical and electrical parameters of the substrate [27]. The effect of the underpass is taken into account by considering a section of coupled microstrip lines: the underpass is considered as the ground plane and length of the microstrip section corresponds to the width of the underpass. Obtaining the S-parameters of all the sections, the S-matrices are transformed into Y-matrices and connected together to form the inductor.

This model has first been validated for low-value inductors with a strip width (W) and a strip spacing (S), both equal to 16 μm. When the distance between the outer strip of the spiral inductor and the coplanar ground plane, needed for on-wafer measurement purposes, is of the same order of magnitude as the spacing between strips, the effect of the ground plane has to be taken into account, as shown in [26]. In order to avoid this problem, the coplanar waveguide (CPW) ground plane–outer inductor strip distance has been taken large enough ($5 \times W$) for the validation of the new model presented in this paper.

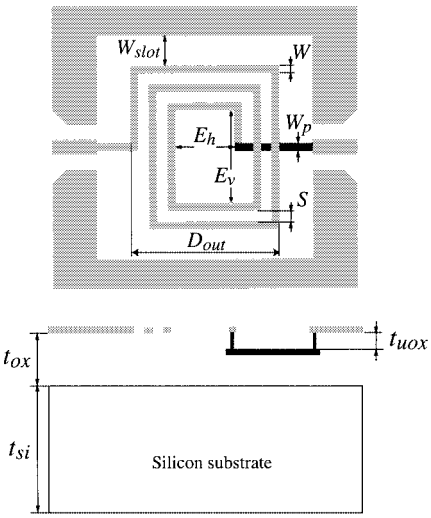

Fig. 1. Top view and cross section of analyzed inductors.

IV. Efficiency and Limitations of the Preliminary Model

The model presented above adequately predicts for spiral, as well as meander inductors: the inductance and quality factor of inductors below and above the resonant frequency, the self-resonant frequency due to the underpass capacitor, as well as the second resonant frequency due to the line length (when the total line length approaches a quarter-wavelength), and the parasitic effects due to the ground planes, if the distance between the coplanar ground planes and the outer strip is lower than $5 \times W$. Furthermore, this model is valid for low-loss dielectric substrates, as well as for low-resistivity substrates such as silicon, and is well adapted for the design due to its short computation time. However, this model suffers from limitations, the most important being the degradation of the precision of the simulated inductance for high W/S ratios, as will be shown in Section VI. This is due to the fact that only the adjacent lines are taken into account for the evaluation of the coupled-line parameters. It has been proven [28] that the impact of the lines located across the hole in the middle of the inductor is not negligible; they introduce a negative coupling due to the opposite direction of the current flowing in the strips. This effect is not taken into account by the preliminary model [1]. Section V shows how the model can be optimized.

V. Improved Model

For RF and microwave low-noise amplifiers and oscillators, the design of high-value inductors with a high-quality factor is needed. This needs a large number of turns and a small distance between the strips. Reducing the distance between the strips, it becomes important to take into account the effect of nonadjacent lines: the full coupling matrix of n coupled lines has to be evaluated, including not only all the lines being on the same side of the inductor, but also the ones located at the opposite side of

TABLE I
GEOMETRICAL DIMENSIONS OF ANALYZED SPIRAL INDUCTORS

Label	n	$W[\mu m]$	$S[\mu m]$	$W_p[\mu m]$	$E_h[\mu m]$	$E_v[\mu m]$	$Length[\mu m]$	$D_{out}[\mu m]$
35T	3.5	10	1	5	50	50	1266	136
45TS5	4.5	10	5	5	50	50	2098	190
45TEH10	4.5	10	1	5	10	90	1826	198
45TEH30	4.5	10	1	5	30	70	1826	178
55T	5.5	10	1	5	50	50	2472	180
85T	8.5	10	1	5	50	50	4942	246
35TCsT	3.5	10	1	5	289	289	4612	375
45TCsT	4.5	10	1	5	141	141	3464	249
$W_{slot} = 50\mu m$								

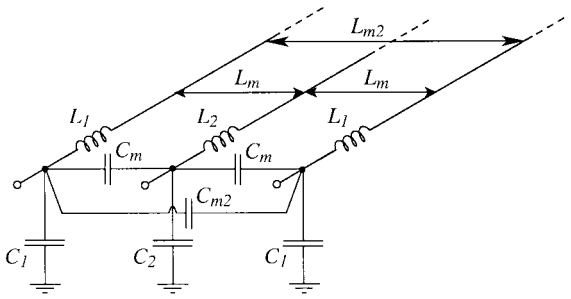

Fig. 2. Equivalent circuit of three coupled microstrip lines. For clarity purposes, the equivalent resistances and conductances in series and parallel with the inductive and capacitive elements, respectively, are not shown.

the middle hole of the spiral. However, the number of parameters increases rapidly and should become prohibitive for a large number of turns.

In order to limit the complexity of the model and then the computation time, it would be interesting to identify the negligible distributed parameters for a spiral inductor. For this purpose, the evaluation of the full coupling matrices of three and four coupled lines of 10-μm width, separated by 1 μm, has been performed and analyzed. This corresponds to the geometry of the spiral inductors used for the inductor model validation. The full analytical analysis of coupled lines has been limited to three and four coupled lines to keep the expressions readable, but of course, the conclusions drawn below are valid for networks with over four coupled lines. Several measurements and simulations comparisons presented in Section VI demonstrate the validity of simplifications described below for inductor structures composed of 3.5 up to 8.5 turns. Fig. 2 shows the complete equivalent lumped circuit for three coupled transmission lines. The symmetry of the structure imposes the equality of the lineic parameters of the first and third lines, as well as their coupling parameters with the central line. Our model takes into account the ohmic and dielectric loss, but for clarity purposes, the equivalent series resistances (R_i) and parallel conductances (G_i) are not included in Fig. 2. Explanations about conductor and dielectric loss modeling are given below. In the frequency domain, the differential equations describing the evolution of the voltage and current along the lines are

$$\begin{aligned}
\frac{dI_1(z)}{dz} &= -j\omega C_1 V_1(z) - j\omega C_m\big(V_1(z) - V_2(z)\big) \\
&\quad - j\omega C_{m2}\big(V_1(z) - V_3(z)\big) \\
\frac{dI_2(z)}{dz} &= -j\omega C_2 V_2(z) - j\omega C_m\big(V_2(z) - V_1(z)\big) \\
&\quad - j\omega C_m\big(V_2(z) - V_3(z)\big) \\
\frac{dI_3(z)}{dz} &= -j\omega C_1 V_3(z) - j\omega C_m\big(V_3(z) - V_2(z)\big) \\
&\quad - j\omega C_{m2}\big(V_3(z) - V_1(z)\big) \\
\frac{dV_1(z)}{dz} &= -j\omega L_1 I_1(z) - j\omega L_m I_2(z) - j\omega L_{m2} I_3(z) \\
\frac{dV_2(z)}{dz} &= -j\omega L_2 I_2(z) - j\omega L_m I_1(z) - j\omega L_m I_3(z) \\
\frac{dV_3(z)}{dz} &= -j\omega L_1 I_3(z) - j\omega L_m I_1(z) - j\omega L_{m2} I_1(z).
\end{aligned} \tag{1}$$

Deriving the three last equations versus z gives the following equation system:

$$\begin{aligned}
\frac{d^2V_1(z)}{dz^2} &= C_{11}V_1(z) + C_{12}V_2(z) + C_{13}V_3(z) \\
\frac{d^2V_2(z)}{dz^2} &= C_{21}V_1(z) + C_{22}V_2(z) + C_{21}V_3(z) \\
\frac{d^2V_3(z)}{dz^2} &= C_{13}V_1(z) + C_{12}V_2(z) + C_{11}V_3(z)
\end{aligned} \tag{2}$$

with

$$\begin{aligned}
C_{11} &= \omega^2(-L_1C_m - L_1C_{m2} + L_mC_m \\
&\qquad + L_{m2}C_{m2} - L_1C_1) \\
C_{12} &= \omega^2(L_1C_m + L_{m2}C_m \\
&\qquad - L_mC_2 - 2L_mC_m) \\
C_{13} &= \omega^2(-L_{m2}C_{m2} + L_1C_{m2} + L_mC_m \\
&\qquad - L_{m2}C_1 - L_{m2}C_m) \\
C_{21} &= \omega^2(L_2C_m - L_mC_m - L_mC_1) \\
C_{22} &= \omega^2(2L_mC_m - 2L_2C_m - L_2C_2)
\end{aligned} \tag{3}$$

Assuming propagation along the z-axis $(-j\beta z)$, solving (3) reduces to the evaluation of eigenvalues and eigenvectors [29] for voltage or for current as follows:

$$\begin{bmatrix} C_{11} & C_{12} & C_{13} \\ C_{21} & C_{22} & C_{21} \\ C_{13} & C_{12} & C_{11} \end{bmatrix} \begin{bmatrix} V_1 \\ V_2 \\ V_3 \end{bmatrix} = -\beta^2 \begin{bmatrix} V_1 \\ V_2 \\ V_3 \end{bmatrix} \tag{4}$$

$$\begin{bmatrix} C_{11} & C_{12} & C_{13} \\ C_{21} & C_{22} & C_{21} \\ C_{13} & C_{12} & C_{11} \end{bmatrix} \begin{bmatrix} I_1 \\ I_2 \\ I_3 \end{bmatrix} = -\beta^2 \begin{bmatrix} I_1 \\ I_2 \\ I_3 \end{bmatrix}. \tag{5}$$

The three eigenvectors of (4), as well as their eigenvalues are evaluated by the variational principle developed at the laboratory [27]. Inserting them in (5) gives a system of five independent equations with the five unknowns C_{11}, C_{22}, C_{12}, C_{21}, and C_{13}. The next step is the calculation of the lineic parameters by

TABLE II
SIMULATED VALUES OF THE LINEIC CAPACITANCES IN pF/m AND INDUCTANCES IN $\mu H/m$ OF THREE COUPLED LINES WITH $W = 10\ \mu m$, $S = 1\ \mu m$, $t_{ox} = 4\ \mu m$, $t_{si} = 500\ \mu m$, AND $\rho_{si} = 20\ \Omega \cdot$ cm

Capacitance	Direct extraction	Silvaco	Proposed model	Inductance	Proposed model
C_1	110	29.5	31	L_1	1.16
C_2	44.6	3	0	L_2	1.4
C_m	59.5	170	173	L_m	1.04
C_{m2}	-8	6	0	L_{m2}	0.76

(3). This is, however, a system of five equations with eight unknowns. Three other equations have to be added to find out all the parameters. These equations are obtained by expressing the power for the three propagation modes

$$P_1 = \omega \frac{L_1 + L_{m2} + (C_{21})^2 L_2/2 + 2L_m C_{21}}{\beta_1}$$
$$P_2 = \omega \frac{L_1 + L_{m2} + (C_{22})^2 L_2/2 + 2L_m C_{22}}{\beta_2} \quad (6)$$
$$P_3 = \omega \frac{L_1 - L_{m2}}{\beta_3}.$$

The lineic parameters are then extracted from (3) and (6). The extraction of all the line parameters L_1, L_2, L_m, L_{m2}, C_1, C_2, C_m, and C_{m2} is, however, not straightforward because they appear as products in (3) and the possibility to recover them depends on their respective order of magnitude, which is directly related to the geometry of the coupled lines. It is then necessary to perform a preliminary evaluation of the line parameters, especially the capacitances. Their values, given in Table II, have been obtained by using a commercial 2-D simulator Silvaco[1] and extracted from our multiline analysis.

Due to the large distance h between the lines and ground plane, only C_1 has to be taken into account. Actually, C_1 is significantly higher than C_2 due to the important fringing capacitance associated with outer strips. The high aspect ratio of the coupled lines ($W/S = 10$) involves a high value for C_m, which is the dominant element, and a negligible value for the coupling capacitance between nonadjacent elements (C_{m2}). These conclusions are also valid for four-coupled lines: only capacitances between the external lines and the ground plane and capacitances between adjacent strips have to be considered. As a consequence, C_2 and C_{m2} are too small to be accurately extracted from (3), as shown in Table II under the "Direct extraction" column. The other coupling parameters (L_1, L_2, L_m, L_{m2}, C_1, and C_m) are then extracted from (3) and (6), and their values are given in Table II. In practice, C_2 and C_{m2} will be fixed to zero. It is clear from the measurements that all the inductive couplings are in the same order of magnitude, even for the nonadjacent lines, and then none can be neglected. This has been checked by applying a sensitivity analysis to the model and has also been proven by Shepherd in [28].

This preliminary step is necessary in order to avoid trying to extract capacitances that are so small that the calculated S-parameters are completely insensitive to their value.

The next step is the analysis of the integrated inductor. The inductor is divided into sections of coupled lines, as represented in Fig. 3. As mentioned before, the capacitive coupling takes into account the coupling with the adjacent lines only, and the inductive coupling takes into account all the lines, including those extending across the gap. The sign of the mutual inductors between two lines depends, of course, on the respective direction of the current flow.

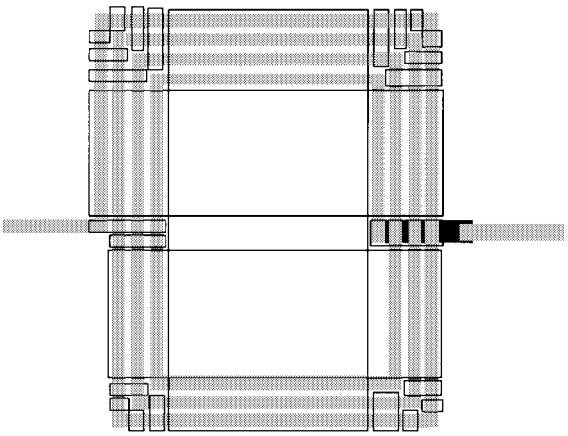

Fig. 3. Division of the spiral inductor into sections of coupled microstrip lines for the improved model.

In the model, the conductor and dielectric losses are both taken into account. In a few words, the technique assumes a realistic distribution of current on the strips, from which an accurate value of the complex propagation constant associated to each coupled mode is derived, together with the modal electric- and magnetic-field distribution in each dielectric lossy layer. Knowing the modal field distribution and associated complex propagation constant, the modal power under the dielectric losses' assumption is derived. Modal values of complex propagation constant γ and associated power P are inserted into (3) and (6) in the case of a three-line section, for example, and lineic L_i-, G_i-, and C_i-parameters are deduced. Next, the series lineic resistance R_i of each strip is computed according to [25], taking into account the skin-effect limitation.

The model also takes into account the presence of eddy currents inside the lossy multilayered substrate. This is demonstrated by several simulation results compared to experimental data in Section VI.

Fig. 4 shows schematically the simulation procedure from the geometrical and electrical characteristics of a given spiral inductor (inputs) to the inductor S-parameters or a lumped equivalent circuit (outputs) computed by the new simulator. These outputs can then be used by a microwave circuit designer to optimize the RF IC performance.

VI. VALIDATION OF THE NEW MODEL

The measurement of a battery of inductors (Table I) implemented on quartz and moderate-resistivity silicon substrates has validated this new model.

[1]Silvaco Int., Santa Clara, CA, 1999.

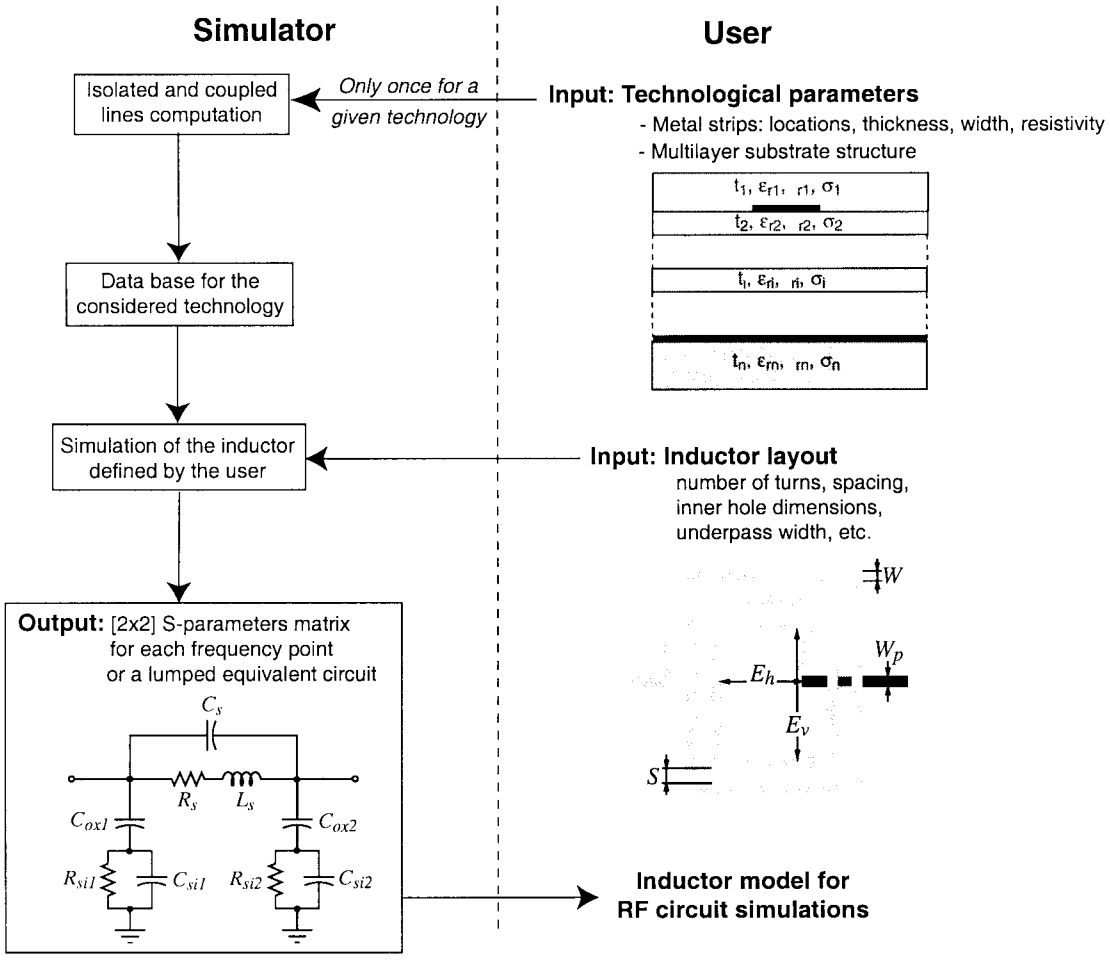

Fig. 4. Simulation procedure: from the technological inputs and inductor layout to the high-frequency simulated characteristics of the inductor.

Fig. 5 shows the comparison between measured and simulated S-parameters of the 55T inductor; the improvements of the new model clearly appear. Table III compares the measured values of the inductance and the self-resonant frequency to the values calculated by the preliminary model [1] and by the new one. The preliminary model systematically overestimates the value of the inductance by neglecting the negative coupling due to the current across the hole in the middle of the inductor structure and, as a consequence, gives only an approximate value of the self-resonant frequency. It is important to accurately predict the self-resonant frequency because its value decreases for increasing value of inductance so that there is a risk for high-L and high-Q inductors to have a self-resonant frequency coming close to the working frequency. Most of the models in the literature are not adequate; they usually highly overestimate the resonant frequency.

The measurements in Table III (inductors 45TEH10 and 45TEH30) show that the inductance increases when the size of the hole in the middle of the spiral increases (increasing E_h). The new model predicts well this increase, whereas the preliminary one does not because it does not take into account the negative mutual inductance between lines in which the current flows in the opposite direction.

Fig. 6 shows the good agreement between measured and simulated S-parameters over the whole frequency range from 0.04 to 40 GHz for an inductor (55T) built on two different substrates. These results demonstrate the efficiency of the modeling procedure to evaluate accurately the substrate effects for moderate resistivity [silicon of 20 Ω·cm, see Fig. 6(a)] or extremely high-resistivity substrates [quartz, see Fig. 6(b)]. If we look at little bit closer at the S_{21}-parameter, an increase of the error between simulations and measurements can be observed for the inductor lying on the silicon substrate, mainly above the self-resonant frequency (around 20 GHz for 55T). We would like to stress the fact that no optimization of the structure parameters have been used in order to fit with the measurements. The electrical parameters for the silicon substrate (permittivity and resistivity) and the physical dimensions of the various layers (oxide, silicon, metal, etc.) provided by the foundry, as well as the strips characteristics (width and spacing) only have been introduced in the simulator. In order to see how sensitive the magnitude and phase of the S_{21}-parameter are versus substrate and conductor losses, the inductor has been simulated with the data provided by the foundry, cancelling the conductor loss, increasing the oxide layer under the spiral inductor, and increasing the silicon substrate resistivity. The results demonstrate that the effect of conductor losses appears mainly on the magnitude of S_{21} below the self-resonant frequency, whereas the silicon substrate losses (intrinsic silicon substrate resistivity and thickness of the oxide layer) have an impact on the S_{21} phase mainly above the in-

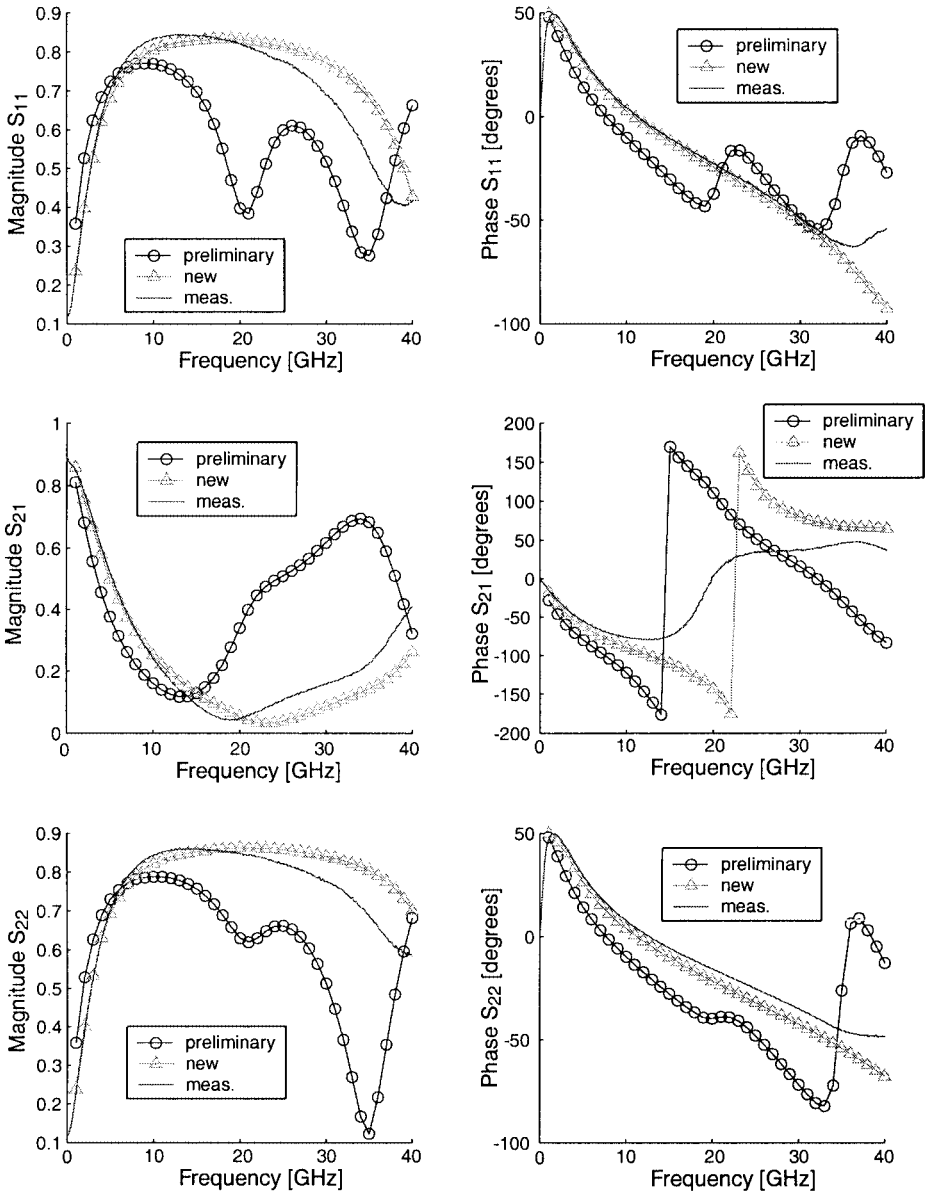

Fig. 5. Comparison between measured and simulated S-parameters for a square spiral inductor of 5.5 turns (called 55T in Table I).

TABLE III
COMPARISON BETWEEN MEASURED INDUCTANCE AND SELF-RESONANT FREQUENCY, AND SIMULATED ONES BY THE PRELIMINARY AND NEW MODELS FOR INDUCTORS BUILT ON MODERATE-RESISTIVITY SILICON SUBSTRATE

	Measurements		Preliminary Model		New Model	
Label	L [nH]	F_{res} [GHz]	L [nH]	F_{res} [GHz]	L [nH]	F_{res} [GHz]
35T	1.65	37.6	2.46	25	1.8	36
45TS5	2.9	28.6	4.32	20.5	3.1	30
45TEH10	2.51	27	3.88	19.5	2.56	30
45TEH30	2.68	26.1	3.88	19.5	2.74	27
55T	4.14	19.8	5.58	16	4.35	21

ductor self-resonance. A wrong estimation of the silicon resistivity can then explain the disagreement between the measured and simulated S_{21} phase. We are convinced that we could better fit the simulation results with the measurements by simply optimizing the silicon substrate or conductor resistivity and thickness of the oxide layer considered by the simulator. Moreover, we would also like to stress on the fact that the loss mechanisms inside the silicon substrate are modeled in the present model by considering the silicon resistivity of the wafer, i.e., the silicon substrate is viewed as a dielectric with losses. Actually, it has been demonstrated that the losses mechanisms are greatly influenced by the presence of free carriers inside the semiconductor substrate leading to the formation of inversion, accumulation, or depletion layers [30]. Therefore, the presence of these free carriers inside the silicon substrate should be taken into account for improving the modeling of substrate losses. We are currently making simulations and measurements of various microstrip and CPW transmission lines on different silicon sub-

TABLE IV
MEASURED AND SIMULATED INDUCTANCE VALUE, QUALITY FACTOR AND SELF-RESONANT FREQUENCY FOR VARIOUS SPIRAL INDUCTORS

Label	Measurements			Simulations		
	L [nH]	F_{sr} [GHz]	Q_{max}	L [nH]	F_{sr} [GHz]	Q_{max}
35T	1.65	37.6	4.8	1.80	36	5.2
35T_Q	1.74	35	7.24	1.81	36.5	7.47
45TS5	2.9	28.6	3.9	3.1	30	3.5
45TS5_Q	2.89	28.3	7.25	3.17	28	7.67
45TEH10	2.51	27	3.9	2.56	30	4.2
45TEH10_Q	2.63	25.1	5.58	2.45	23	6.6
45TEH30	2.68	26.1	4.08	2.74	27	4.21
45TEH30_Q	2.63	22	6.13	2.8	23	7.04
55T	4.14	19.2	3.8	4.35	21	3.4
55T_Q	4.09	19.8	6	4.25	19	6.9
85T	11.4	9.2	2.75	12.2	10	3.2
85T_Q	11.18	10.9	5.41	12.28	11.2	6.06
35TCsT	9.4	8.4	2.7	10	10	2.5
35TCsT_Q	9.22	8.7	4.55	9.8	9	4.9
45TCsT	6.8	12	3.31	7.4	12.5	3.36
45TCsT_Q	6.7	12.9	6.23	7.2	13	6.26

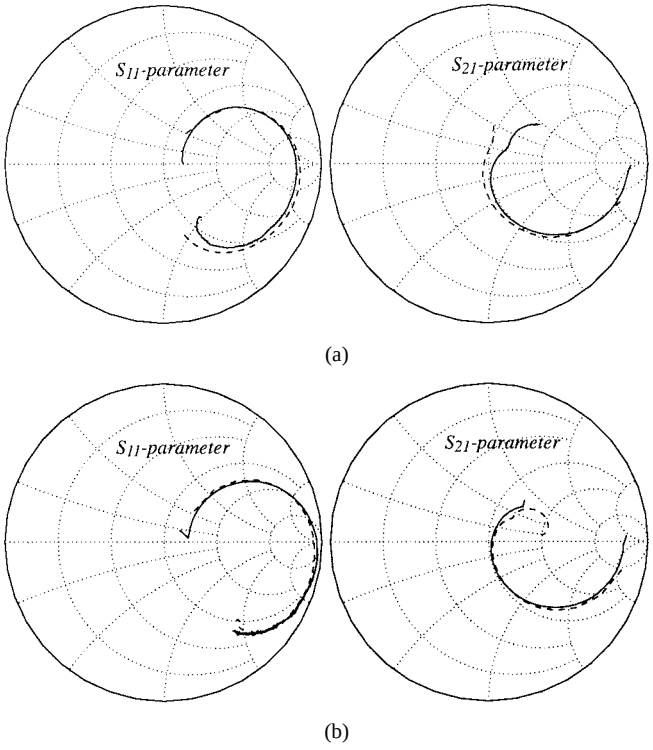

Fig. 6. Measured (continuous line) and simulated (dashed line) S-parameters from 40 MHz to 40 GHz for a square spiral inductor of 5.5 turns (called 55T in Table I) built on: (a) a moderate-resistivity silicon and (b) quartz wafers.

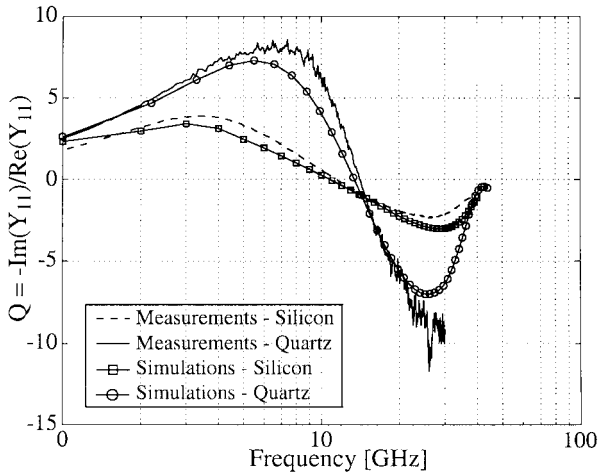

Fig. 7. Measured and simulated quality factor from 40 MHz to 40 GHz for a square spiral inductor of 5.5 turns (called 55T in Table I, Part I) built on quartz and moderate-resistivity silicon wafers.

strates in order to correctly model the silicon substrate behavior over a wide frequency band.

The evolution of the quality factor is most of the time badly predicted or not predicted at all in the literature. The model presented here accurately gives the evolution of the quality factor versus frequency (Fig. 7) and then correctly predicts $Q_{\max}(=\max(-\Im(Y_{11}/\Re(Y_{11}))$, as demonstrated in Table IV.

Yue *et al.* experimentally demonstrate the effects of aluminum ground shields on the equivalent π model parameters of monolithic inductors. Fig. 8 shows the measured inductance presented in [11] for a square spiral inductor composed of seven turns, 15-μm linewidth, and 5-μm line space deposited on a low-resistivity silicon substrate with (SGS) or without a ground shield (NGS). For both designs (SGS and NGS), we can observe a good agreement between our simulations and Yue *et al.*'s measurements. The inductance value is extracted from the measured and simulated Y-parameters by $L = \Im(-1/Y_{12})/\omega$. The large variation of the inductance value versus frequency due to the presence of a solid ground shield is well predicted. Our model can then be used to investigate the effects of heavily doped (10-20 m $\Omega \cdot$ cm) substrates, which are popular silicon substrates for CMOS RF ICs, on the inductors behavior. The simulated inductance value and quality factor of inductor designs, called 35T, 45T, and 55T in this paper, are shown in Fig. 9 for a low-resistivity silicon substrate of 1 $\Omega \cdot$ cm. The simulated values of Q_{max} for these inductors built on a low-resistivity substrate are in accordance with the values given in the literature [31].

Finally, the propagation characteristics (propagation coefficient, attenuation coefficient, and characteristic impedance) for each set of coupled lines are calculated using the variational formalism, which reduce the implicit eigenvalue problem associated to full-wave methods by a simple explicit eigenvalue problem, as described in [27]. This is one of the main advantages of our model. It contributes greatly to the reduction of the

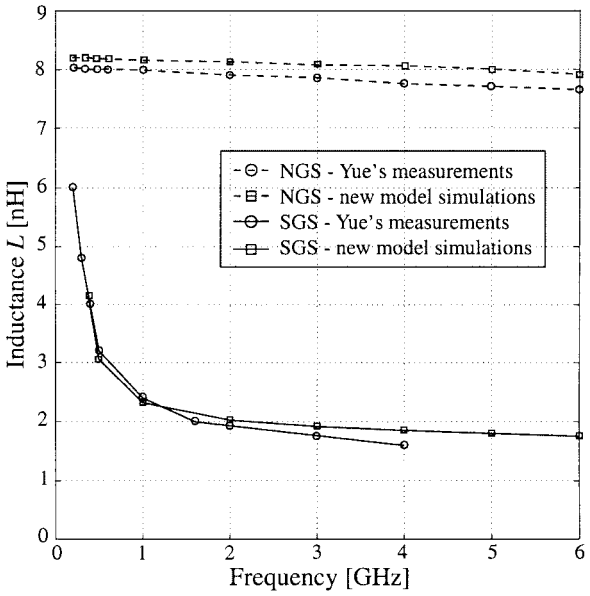

Fig. 8. Measured and simulated inductance for a square spiral inductor built on a moderate-resistivity silicon wafer with (SGS) and without (NGS) a solid ground shield.

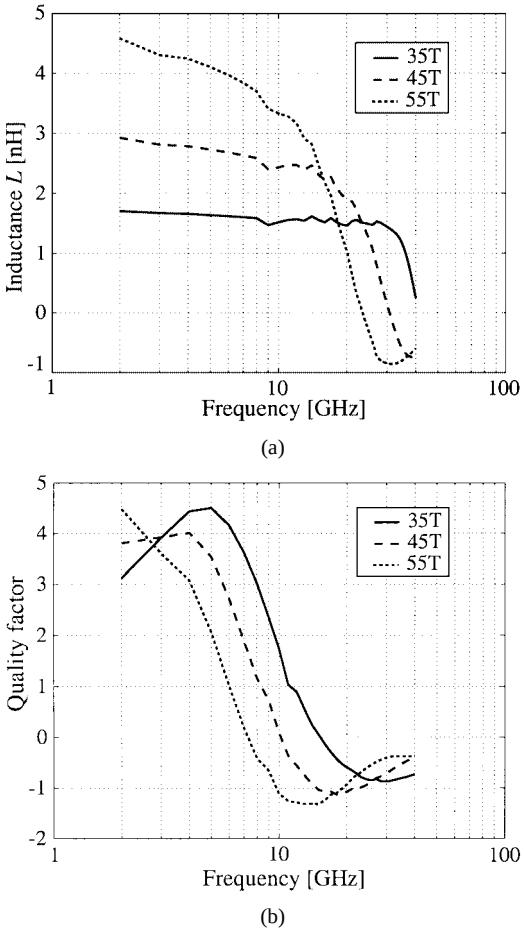

Fig. 9. Simulated inductance value and quality factor for inductors of 3.5, 4.5, and 5.5 turns built on a low-resistivity silicon substrate of 1 $\Omega \cdot$ cm.

simulation time. The simulation time is, of course, increasing with the number of turns, but it stays reasonable for usual spiral inductors. We have observed a computation time of approximately 2-, 5-, and 35-s/frequency point for inductors of 3.5, 5.5, and 8.5 turns, respectively. This has to be compared to the data given by authors in [13]: on a similar computer, a 3-D simulator needs 5 min/frequency point, while the extraction of their own lumped-element π-network requires 2 min/frequency point.

VII. Conclusion

The model presented in this paper has been proven to be an efficient method for designing MMIC inductors built on both insulating and (semi)conducting substrates. Using this new approach, the behavior of the device has been described over a wide-frequency band, with a very reduced numerical complexity, and as function of the geometrical and electrical parameters of the inductor and multilayer substrate only. Hence, the scalability of the proposed model is ensured, which is a main advantage compared with conventional models based on lumped-element equivalent circuits. Results are experimentally validated up to the second self-resonant frequency, showing the efficiency of the model for taking into account wide-band distributed effects. This is of particular interest for nonlinear applications, such as oscillator design, where the value of the terminations are also needed at harmonic frequencies. This new design tool is shown to be useful for analyzing and optimizing inductor topologies.

Acknowledgment

The authors would like to thank the technical staff of the Laboratoire d'electronique et de Technologie de l'information (LETI), Grenoble, France, for building the integrated inductors presented in this paper.

References

[1] D. D. Rathman, J. A. Burns, R. Berger, A. M. Soares, and R. H. Mathews, "High frequency performance of a fully depleted 0.25 ţm SOI CMOS technology," in *IEEE MTT-S Int. Microwave Symp. Dig.*, June 1999, pp. 577–580.

[2] C. Raynaud, O. Faynot, J.-L. Pelloie, F. Martin, S. Tedesco, J. Cluzel, A. Grouillet, B. Dal'zotto, and D. Vanhoenacker, "Scability of fully-depleted SOI technology into 0.13 ţm 1.2 V - 1 V CMOS generation," in *Proc. IEEE Int. SOI Conf.*, Oct. 1999, pp. 86–87.

[3] C. Raynaud, J. Gautier, G. Guegan, M. Lerne, E. Playez, and G. Dambrine, "High-frequency performance of submicrometer channel-length silicon MOSFET's," *IEEE Electron Device Lett.*, vol. 12, pp. 667–669, Dec. 1991.

[4] J.-P. Colinge, *Silicon-on-Insulator Technology: Materials to VLSI*. Norwell, MA: Kluwer, 1997.

[5] D. Schreurs, H. Van Meer, S. Kubicek, J. Lyu, B. Nauwelaers, and K. De Meyer, "Optimization of nMOS high-frequency transistor characteristics for application in MMIC's," in *Silicon Monolithic Integrated Circuits in RF Syst. Dig.*, 1998, pp. 72–76.

[6] K. B. Ashby, I. A. Koullias, W. C. Finley, J. J. Bastek, and S. Moinian, "High Q inductors for wireless applications in a complementary silicon bipolar process," *IEEE J. Solid-State Circuits*, vol. 31, pp. 4–9, Jan. 1996.

[7] H. B. Erzgraber, T.T. Grabolla, H. H. Richter, P. Schley, and A. Wolff, "A novel buried oxide isolation for monolithic RF inductors on silicon," in *IEEE Int. Electron Device Meeting Tech. Dig.*, vol. 8, Dec. 1998, pp. 535–539.

[8] M.-J. Yu, Y.-J. Chan, L.-H. Laih, and J.-W. Hong, "Improved microwave performance of spiral inductors on Si substrates by chemically anodizing a porous silicon layer," *Microwave Opt. Technol. Lett.*, no. 4, pp. 232–234, Aug. 2000.

[9] J.-B. Yoon, C.-H. Han, E.Euisik Yoon, and C.-K.Choong-Ki Kim, "Monolithic high-Q overhang inductors fabricated on silicon and glass substrates," in *IEEE Int. Electron. Devices Meeting Tech. Dig.*, Dec. 1999, pp. 753–756.

[10] J. M.Jose M. Lopez-Villegas, J.Josep Samitier, C.Charles Cane, P.Pere Losantos, and J.Joan Baussels, "Improvement of the quality factor of RF integrated inductors by layout optimization," *IEEE Trans. Microwave Theory Tech.*, vol. 48, pp. 76–83, Jan. 2000.
[11] C. PC Patrick Yue and S. SS. Simon Wong, "On-chip spiral inductors with patterned ground shields for Si-based RF IC's," *IEEE J. Solid-State Circuits*, vol. 33, pp. 743–752, May 1998.
[12] J. N. Burghartz, M. Soyuer, and K. A. Jenkins, " Microwave inductors and capacitors in standard multilevel interconnect silicon technology," *IEEE Trans. Microwave Theory Tech.*, vol. 44, pp. 100–104, Jan. 1996.
[13] J. R. Long and M. A. Copeland, "The modeling, characterization, and design of monolithic inductors for silicon RF IC's," *IEEE J. Solid-State Circuits*, vol. 32, pp. 357–368, Mar. 1997.
[14] F.Francesco Svelto, S.Stefano Deantoni, and R.Rinaldo Castello, "A 1.3 GHz low-phase noise fully tunable CMOS LC VCO," *IEEE J. Solid-State Circuits*, vol. 35, pp. 356–361, Mar. 2000.
[15] C.-Y.Chung-Yu Wu and S. Y.Shuo-Yuan Hsiao, "The design of a 3-V 900-MHz CMOS bandpass amplifier," *IEEE J. Solid-State Circuits*, vol. 32, pp. 159–167, Feb. 1997.
[16] A.Ahmadreza Rofougaran, J. Y.-C.James Y.-C. Chang, M.Maryam Rofougaran, and A. A.Asad A. Abidi, "A 1 GHz CMOS RF front-end IC for a direct-conversion wireless receiver," *IEEE J. Solid-State Circuits*, vol. 31, pp. 880–889, July 1996.
[17] J.Jan Craninckx and M. S. J.Michiel S. J. Steyaert, "A 1.8-GHz low-phase-noise CMOS VCO using optimized hollow spiral inductors," *IEEE J. Solid-State Circuits*, vol. 32, pp. 736–744, May 1997.
[18] M. Goffioul, J.-P. Raskin, and D. Vanhoenacker, "Microwave integrated CMOS oscillators on Silicon-on-Insulator substrate," presented at the 30th Eur. Microwave Conf., Oct. 2000.
[19] V. Tripathy and H. Lee, " Spectral-domain computation of characteristic impedances and multiport parameters of multiple coupled microstrip lines," *IEEE Trans. Microwave Theory Tech.*, vol. 37, pp. 215–220, Jan. 1989.
[20] J. M. C. J. Mautz C. Wei, R. F. Harrington, and T. Sarkar, "Multiconductor transmission lines in multilayered dielectric media," *IEEE Trans. Microwave Theory Tech.*, vol. MTT-32, pp. 439–450, Apr. 1984.
[21] Z. Chen and B. Gao, "Full-wave analysis of multiconductor coupled lines in MIC's by the method of lines," in *Proc. Inst. Elect. Eng.*, vol. 136, Oct. 1989, pp. 399–404.
[22] P. Daly, "Hybrid-mode, analysis of microstrip by finite element method," *IEEE Trans. Microwave Theory Tech.*, vol. 19, pp. 19–25, Jan. 1971.
[23] J. Crols, P. Kinget, J. Craninckx, and M. Steyeart, "An analytical model of planar inductors on lowly doped silicon substrates for analog design up to 3 GHz," in *VLSI Circuits Symp. Tech. Dig.*, 1996, pp. ???–???.
[24] J. Lau, T. H. Lee, S. S. Wong, C. P. Yue, and C. Ryu, "A physical model for planar spiral inductors on silicon," in *Proc. Int. Electron Devices Meeting Tech. Dig.*, 1996.
[25] H. M. Greenhouse, "Design of planar rectangular microelectronic inductors," *IEEE Trans. Parts, Hybrids, Packag.*, pp. 101–109, June 1974.
[26] I. Huynen, "Novel fast multiline analysis of parasitic effects in CPW inductors for MMIC's," *IEEE Microwave Guided Wave Lett.*, vol. 8, pp. 72–74, Feb. 1998.
[27] I. Huynen, D. Vanhoenacker-Janvier, and A. Vander Vorst, "Spectral domain form of new variational expression for very fast calculation of multilayered lossy planar line parameters," *IEEE Trans. Microwave Theory Tech.*, vol. 42, pp. 2099–2106, Nov. 1994.
[28] P. R. Shepherd, "Analysis of square-spiral inductors for use in MMIC's," *IEEE Trans. Microwave Theory Tech.*, vol. MTT-32, pp. 467–472, Apr. 1984.
[29] J. Malherbe, *Microwave Transmission Line Filters*. Norwood, MA: Artech House, 1979, p. 334.
[30] J.-P. Raskin, A. Viviani, D. Flandre, and J.-P. Colinge, "Substrate crosstalk reduction using SOI technology," *IEEE Trans. Electron Devices*, vol. 44, pp. 2252–2261, Dec. 1997.
[31] D. Lovelace, N. Camilleri, and G. Kannell, "Silicon MMIC inductor modeling for high volume, low cost applications," *Microwave J.*, pp. 60–71, Aug. 1994.

Morin Dehan was born in Charleroi, Belgium, in 1977. He received the Industrial Engineer degree from the Institut Supérieur Industriel Catholique du Hainaut (ISICHt), Charleroi, Belgium, in 1998,and is currently working toward the Ph.D. degree in electronic engineering from the Université catholique de Louvain (UCL), Louvain-la-Neuve, Belgium.

Since 1999, he has been with the Microwave Laboratory (EMIC), UCL. His main research concerns the modeling and characterization of integrated devices at microwave frequencies.

Jean-Pierre Raskin (M'97) was born in Aye, Belgium, in 1971. He received the Industrial Engineer degree from the Institut Supérieur Industriel d'Arlon, Arlon, Belgium, in 1993, and the B.S. and Ph.D. degrees in applied sciences from the Université catholique de Louvain, Louvain-la-Neuve, Belgium, in 1994 and 1997, respectively.

In 1998, he joined the Electrical Engineering and Computer Science Department, The University of Michigan, at Ann Arbor. He has been involved in the development and characterization of micromachining fabrication techniques for microwave and millimeter-wave circuits and microelectromechanical transducers/amplifiers working in hard environments. Since January 2000, he has been an Associate Professor with the Microwave Laboratory, Université catholique de Louvain. He is also a member of the Research Center in Micro and Nanoscopic Materials and Electronic Devices, Université catholique de Louvain. He has authored or coauthored over 80 scientific papers. His research interests are the modeling, characterization, and fabrication of SOI MOSFETs for RF and microwave applications, planar circuits at millimeter and sub-millimeter waves frequencies, RF microelectromechanical systems (MEMS), and micromachined sensors.

Isabelle Huynen (S'87–A'95–M'96) was born in Brussels, Belgium, in 1965. She received the Electrical Engineer degree and Ph.D. degree in applied sciences from the Université Catholique de Louvain (UCL), Louvain-la-Neuve, Belgium, in 1989 and 1994, respectively.

In 1989, she joined the Microwave Laboratory, UCL, where she is currently a Research Associate of the National Fund for Scientific Research (FNRS), Belgium, and a Part-Time Associate Professor. Her main research deals with electromagnetic theory and measurement techniques applied to materials, devices, and circuits at microwave, millimeter-wave, and optical wavelengths. She has particular interest in the development of microwave and millimeter-wave devices based on nanoscaled materials and topologies, in view of synthesizing wide-band hybrid and integrated opto-electronic circuits for telecommunications and applications.

Dr. Huynen is a member of the Belgian Society of Telecommunication and Electronic Engineers (SITEL) and the Royal Society of Belgian Electricians (SRBE/KVBE).

Danielle Vanhoenacker-Javier (M'88–SM'90) received the Electrical Engineer degree and Ph.D. degree in applied sciences from the Université catholique de Louvain (UCL), Louvain-la-Neuve, Belgium, in 1978 and 1987, respectively.

She is currently with the UCL, where she was an Assistant (1979–1987), Senior Scientist (1987–1994), Associate Professor (1994–2000), and Professor (since 2000) with the Microwave Laboratory. Since 2001, she has been Head of the Microwave Laboratory. She has been involved in the study of atmospheric effects on propagation above 10 GHz for over 25 years and she is now interested in the analysis and modeling of the mobile propagation channel and the evaluation of its impact on communication systems. In 1989, she extended her research activity to microwave circuits. She is involved in the analysis, design, and measurement of microwave planar passive and active circuits with a special interest, since 1994, in microwave ICs on SOI. She has authored over 120 technical papers and coauthored a book.

Dr. Vanhoenacker-Janvier is reviewer for various international conferences and IEEE and Institution of Electrical Engineers (IEE), U.K., journals. She is also a member of evaluation committees for grants and projects at Innovatie door Wetenschap en Technologie (IWT) since 1997, and at Fonds door Wetenschappelijk Onderzoek (FWO) and Fonds pour la formation a la Recherche dans l'Industrie et l'Agriculture (FRIA) since 2001.